# Ferroelectric-driven tunable magnetism in ultrathin platinum films

Qilong Sun,[1,*] Farzad Mahfouzi,[1] Julian P. Velev,[2] Evgeny Y. Tsymbal,[3] and Nicholas Kioussis[1,†]

[1]*Department of Physics and Astronomy, California State University, Northridge, California 91330, USA*

[2]*Department of Physics, University of Puerto Rico, San Juan, Puerto Rico 00931, USA*

[3]*Department of Physics and Astronomy and Nebraska Center for Materials and Nanoscience, University of Nebraska, Lincoln, Nebraska 68588-0299, USA*

(Received 22 April 2020; accepted 17 November 2020; published 2 December 2020)

Electric control of magnetism in magnetoelectric (ME) multiferroics is expected to have a significant impact on a wide range of technological applications. Here, we predict the modulation of magnetism in ultrathin platinum films due to the ferroelectric polarization of the $BaTiO_3$ substrate, which along with biaxial strain changes the density of states at the Fermi energy. We demonstrate that both the magnitude and direction of the magnetization depend strongly on the polarization direction and/or strain. This leads to an unprecedented ME effect involving a giant change of magnetocrystalline anisotropy under polarization switching due to the large spin-orbit coupling of Pt. These findings pave the way of an alternative strategy for the design of nonvolatile and ultralow power spintronics and magnetic memory storage devices.

DOI: 10.1103/PhysRevMaterials.4.124401

## I. INTRODUCTION

Electric field control of magnetism in magnetoelectric multiferroics (MFs) [1–4], as opposed to current-driven magnetization switching via the spin transfer [5,6] or spin-orbit torque [7,8], is expected to have a significant impact on the design of nonvolatile, ultralow power and highly scalable nanoelectronic and spintronic devices. MFs combining several ferroic orders allow manipulation of one order via the conjugate field associated with a different ferroic order [1,2]. However, the tendency for mutual exclusivity of ferroelectricity (FE) and ferromagnetism (FM) in nature results in the scarcity of single phase multiferroics [9]. The weak magnetoelectric coupling (MEC) and weak spontaneous magnetization/polarization of existing single-phase MFs at room temperature hamper their practical applications [1,2]. To overcome these limitations a great amount of efforts have been oriented towards artificial MFs consisting of FM/FE heterostructures with atomically smooth interfaces [1,2,10,11]. The robust room-temperature MEC in composite MFs along with advances in controlled epitaxial and self-assembly processes have allowed the electric-field control of various magnetic properties, such as the magnetocrystalline anisotropy (MCA) [12,13], the exchange bias [14], and the spin transport [15].

Among the ferroelectrics, $BaTiO_3$ (BTO) is considered a prototype system to explore the strain-mediated ME effect since it undergoes several structural phase transitions as a function of temperature [16]. In addition, BTO can retain the out-of-plane ferroelectricity even in nanometer-thick films [17]. For the magnetic systems, $La_{2/3}Sr_{1/3}MnO_3$ [4], $Fe_3O_4$ [18], Fe [10,13,16], and $CoFe_2O_4$ [19,20] are the most extensively investigated in BTO/FM heterostructures. Here, several underlying atomistic mechanisms for the MEC in composite MFs have been proposed, including interface strain [13,21,22], interface bonding configuration [23–25], accumulation/depletion of spin polarized charge [26], and exchange coupling [10].

Bulk platinum is regarded as a strongly exchange-enhanced paramagnetic metal which nearly satisfies the Stoner criterion [27], $IN(E_F) > 1$, where $I$ and $N(E_F)$ are the exchange integral and density of states at the Fermi energy, respectively. Thus, relatively weak perturbations in the electronic structure may lead to the emergence of incipient ferromagnetism [28]. These include (i) magnetic proximity effect at the interface with a FM metal or insulator [29], (ii) reduction of dimensionality at the surface or nanoparticles/clusters resulting in bandwidth narrowing [30], (iii) biaxial strain [31], and (iv) application of an external electric field via an ionic liquid giving rise to the anomalous Hall effect (AHE) [32,33]. Equally important is the large spin-orbit coupling (SOC) of Pt, compared to its $3d$ or $4d$ counterparts, which has been used for spin-orbit torque magnetization switching.

In this work, employing first-principles calculations, we predict the emergence of magnetism in ultrathin platinum films due to the interfacial effect and ferroelectric polarization of the BTO substrate. We demonstrate that both the magnitude and direction of the magnetization depend strongly on the polarization direction and biaxial strain. The calculations reveal a giant MEC compared to the $3d$ FM/BTO counterparts due to the large SOC of Pt. We elucidate that the underlying mechanism of the giant MEC is the rigid shift of chemical potential. The FE-driven magnetoelectric effects at the Pt/BTO interfaces may be a feasible alternative towards low power and higher speed spintronic devices.

*long.q.sun@gmail.com

†nick.kioussis@csun.edu

 

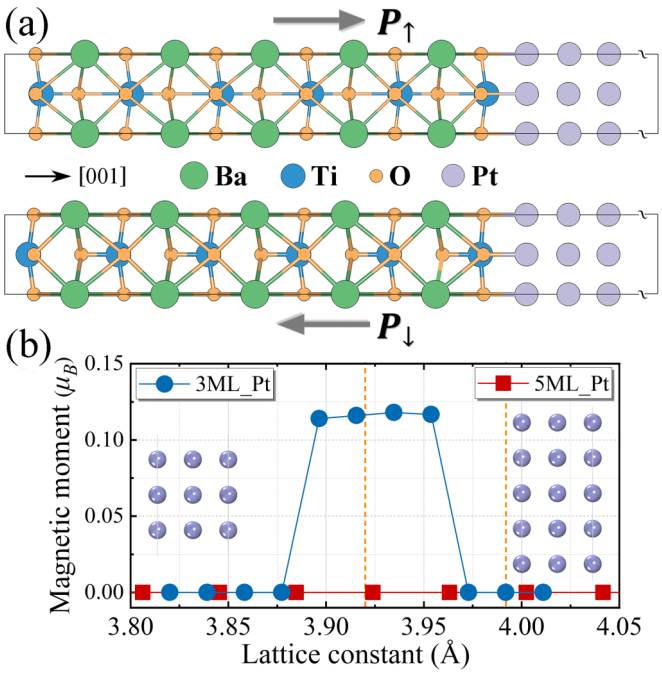


FIG. 1. (a) Atomic structures of the (001) 3Pt/BTO bilayer. The top (bottom) panel shows the interface in which the direction of polarization (gray arrow) $P_\uparrow$ ($P_\downarrow$) is pointing towards (away from) the Pt layer. (b) Average magnetic moment per atom of the 3 and 5 ML freestanding Pt films as a function of in-plane lattice constant. The orange dashed vertical lines denote the experimental lattice constant of bulk BTO (3.992 Å) and Pt (3.920 Å), respectively.

## II. METHODOLOGY

Density functional theory (DFT) calculations within the projector augmented-wave (PAW) method [34] were carried out using the Vienna *ab initio* simulation package (VASP) [35]. The generalized gradient approximation was used to describe the exchange-correlation functional as parametrized by Perdew *et al.* [36], which provides a more accurate treatment of magnetic properties [37,38]. Figure 1(a) shows the slab supercell for the 3Pt/BTO bilayer, consisting of three monolayers (MLs) of fcc Pt on top of five unit cells of tetragonal BTO. The O atoms at the $TiO_2$-terminated interface are placed atop the Pt atoms, which is the most stable stacking configuration [39,40]. A 15 Å vacuum region is adopted to separate the periodic slabs and the dipole corrections are taken into account along the [001] direction. We use a plane-wave cutoff energy of 500 eV and a $12 \times 12 \times 1$ Brillouin zone **k** mesh for the relaxation calculations until the largest force becomes less than $10^{-2}$ eV/Å. In order to study the effect of biaxial strain we have carried out calculations with the in-plane lattice constant, $a_\parallel$, of 3.992 and 3.920 Å corresponding to the experimental lattice constants of bulk BTO and Pt, respectively [41]. The calculated $a_\parallel$ values of 4.00 Å and 3.97 Å for bulk BTO and Pt, respectively, are in good agreement with experiment, even though there is an inherent strain for Pt. The values of the $c/a$ tetragonal distortion of bulk BTO corresponding to the two in-plane lattice constants are 1.01 and 1.12, respectively [22,42]. The three bottom-most BTO unit cells were kept frozen at their equilibrium bulk positions to retain the polarization while the other atoms were fully relaxed. In addition, we find that the position of the Fermi level of the Pt/BTO slab is below the conduction band minimum, ensuring the absence of interfacial band offset error in the FE/metal devices [43]. For the MCA calculations, the SOC was included with a $24 \times 24 \times 1$ **k**-point mesh. The MCA per unit interfacial area is determined from $E_{\mathrm{MCA}} = (E_{[100]} - E_{[001]})/A$, where $E_{[100]}$ and $E_{[001]}$ denote the total energy with in-plane and out-of-plane magnetization, respectively, and $A$ is the in-plane area of the unit cell.

## III. RESULTS AND DISCUSSION

Epitaxial strain has been shown to have a dramatic influence on the emergence of magnetism on ultrathin heavy metals (HMs) layers [31]. Therefore, we first focus on the freestanding 3 ML (001) Pt without BTO. Figure 1(b) illustrates the variation of the average magnetic moments per Pt atom versus $a_\parallel$. The onset of magnetism appears for $a_\parallel$ in the range from 3.896 to 3.954 Å, i.e., in the vicinity of the lattice constant of bulk Pt (3.920 Å), where the average magnetic moment is about 0.11 $\mu_B$/Pt. We find that the nonmonotonic change of the bandwidth near the Fermi level (initial increase followed by a decrease) leads to the limitation of onset magnetism in the specific range of $a_\parallel$. The freestanding Pt monolayer has been also found to be FM under a wide range of biaxial strain, with a magnetic moment of 0.67 $\mu_B$/Pt for $a_\parallel = 3.920$ Å, indicating that thinner Pt layers have higher propensity of becoming magnetic [31]. To probe this conjecture, we have also studied the freestanding 5 ML Pt film, which is indeed nonmagnetic in the entire range of $a_\parallel$ as shown in Fig. 1(b). It is important to note that the 3 ML freestanding Pt is nonmagnetic with $a_\parallel = 3.992$ Å (bulk BTO lattice constant). Thus, if the 3Pt/BTO bilayer at this lattice constant becomes magnetic, the magnetism is induced solely from the effect of BTO.

Figure 2(a) shows the layer-resolved magnetic spin moments without the SOC in the proposed 3Pt/BTO heterostructures. Overall, the calculations reveal several important results: (i) The layered-resolved Pt magnetic moments are smaller for 3.920 Å, indicating that there is an interplay between the strain and polarization effects on the magnetic properties, (ii) the magnetic moments decrease from the surface to the interfacial Pt atoms due to the interfacial hybridization between the Pt-derived $d_{z^2}$ ($d_{xz}$ and/or $d_{yz}$) states with O-derived $p_z$ ($p_x$) states, (iii) the response of all Pt atoms upon polarization reversal indicate a large magnetoelectronic response in sharp contrast with the Fe/BTO system where the MEC is confined to the interface [23], (iv) the layer-resolved Pt magnetic moments for $P_\downarrow$ are larger than those for $P_\uparrow$ polarization, and (v) the emergence of magnetism for $a_\parallel = 3.992$ Å, in contrast to the nonmagnetic freestanding 3 ML Pt, demonstrates that its origin lies only on the FE polarization as well as the interfacial effect of BTO. These findings demonstrate that the combination of several competitive factors, i.e., FE-switching derived charger transfer, interfacial hybridization, and strain effect, can trigger and tune the magnetism in nonmagnetic ultrathin Pt layers.

In addition, we have also carried out calculations of the 3Pt/BTO with $a_\parallel = 3.992$ Å while BTO was kept in the cubic

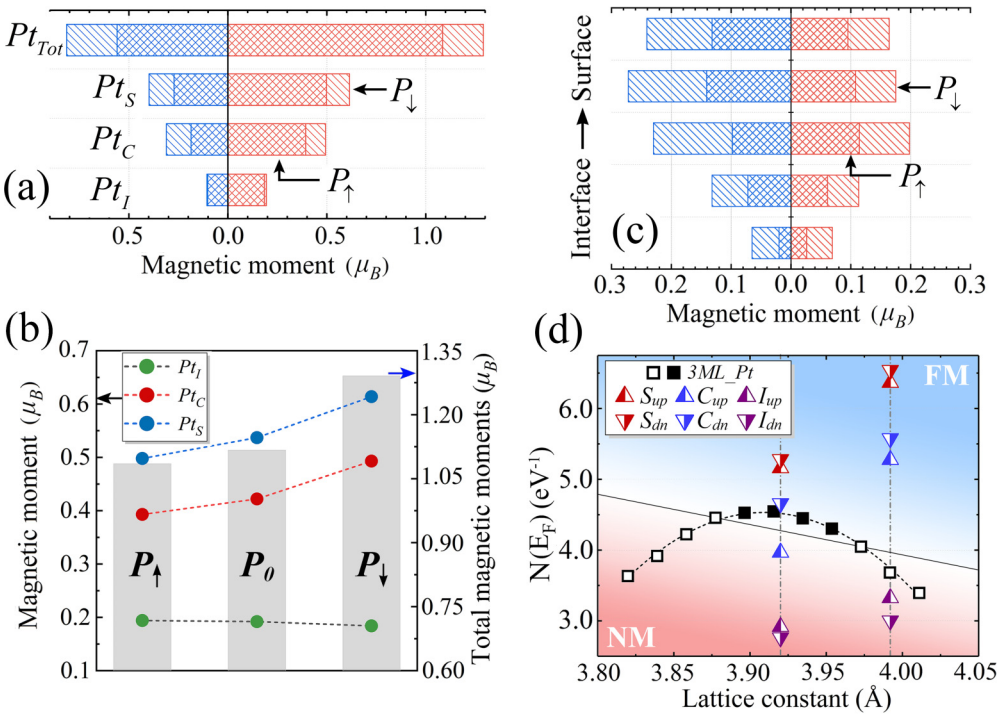


FIG. 2. Layer-resolved magnetic spin moments of the Pt atoms in (a) 3Pt/BTO and (c) 5Pt/BTO for $P_\downarrow$ (single-hatched bar) and $P_\uparrow$ (double-hatched bar) polarizations, and for $a_\parallel = 3.920$ (blue bars) and 3.992 Å (red bars), respectively. The subscripts I, C, and S refer to interface, central, and surface Pt layers, respectively. (b) Variation of the layer-resolved Pt spin moments in the 3Pt/BTO heterostructure with $P_\downarrow$, $P_\uparrow$ and no polarization, $P_0$. The gray bars show the total spin moment of the 3ML Pt film. (d) Non-spin-polarized layer (Pt)-resolved density of states at the Fermi energy [$N(E_F)$] versus $a_\parallel$ for the freestanding 3 ML Pt (black squares) and for the 3Pt/BTO bilayer (triangles) for $P_\uparrow$ ($P_\downarrow$) polarization indicated with the up (down) triangles. The vertical lines denote the experimental lattice constant of bulk BTO (3.992 Å) and Pt (3.920 Å), respectively.

structure without FE distortion. Figure 2(b) shows comparison of the layer-resolved and total magnetic moment for the Pt atoms with $P_\downarrow$, $P_\uparrow$, and $P_0$, where $P_0$ denotes BTO without FE distortion. Interestingly, the calculations reveal the onset of Pt magnetism in the 3Pt/BTO bilayer with $P_0$. This result suggests that the interfacial effect between the Ti-O layer and Pt atoms also contributes to the enhancement of $N(E_F)$, which in turn leads to the magnetization of the Pt atoms. Note that this hybridization-induced contribution to the enhancement of $N(E_F)$ is also present in both $P_\downarrow$ and $P_\uparrow$ polarizations and complements the polarization effect. On the other hand, the magnitude of the Pt magnetic moments for $P_0$ lies between those for $P_\downarrow$ and $P_\uparrow$, except for the interfacial Pt layers ($Pt_I$). This is mainly due to the strong hybridization effect at the interface as discussed above.

Table I lists the relative displacements of the Ti ($d_{\text{Ti-O}}$) and Pt ($d_{Pt_I\text{-O}}$) atoms with respect to the O atoms at the interface of Pt/BTO. Here, the positive (negative) $d_{\text{Ti-O}}$ indicates the Ti displacement towards (away from) the Pt layers. Therefore, larger FE polarization switching will lead to greater changes of the interfacial distance. We also list the total magnetic moment of the Pt film. The changes of magnetic moment upon polarization switching are comparable with those for the Fe/BTO bilayer, even though the Fe atoms have larger spin moments of ~2.67 $\mu_B$ [22].

Since the magnetic moments of all Pt layers undergo a change with polarization reversal, the MEC coefficient $\alpha$ in linear response is given by $\alpha = \dfrac{\mu_0 \Delta M}{E_c}$, where $\mu_0$ is the vacuum permeability, $\Delta M$ is the change of the total magnetization per unit area, and $E_c$ is the coercive electric field to reverse the polarization which in the case of BTO is 100 kV/cm. We find that for Pt/BTO $\alpha$ is $1.93 \times 10^{-10}$ ($1.50 \times 10^{-10}$) Gcm$^2$/V for of 3.920 (3.992 Å), which are of similar order of magnitude as those in Fe/$PbTiO_3$($BaTiO_3$) and $CoFe_2O_4$/$BiFeO_3$ [23,44,45].

In order to investigate the effect of FE polarization on thicker Pt films, we show in Fig. 2(c) the layer-resolved mag-

TABLE I. Values of relative displacements of the Ti ($d_{\text{Ti-O}}$) and Pt ($d_{Pt_I\text{-O}}$) atoms with respect to the O plane at the interface for various 3Pt/BTO. We also list values of total Pt spin magnetic moment, and the MCA, where MCA$^1$ and MCA$^2$ are determined from total energy calculations and the force theorem, respectively.

| | 3.920 (Å) | | 3.992 (Å) | |
|---|---|---|---|---|
| 3Pt/BTO | $P_\uparrow$ | $P_\downarrow$ | $P_\uparrow$ | $P_\downarrow$ |
| $d_{\text{Ti-O}}$ (Å) | 0.262 | −0.154 | 0.087 | −0.047 |
| $d_{Pt_I\text{-O}}$ (Å) | 2.251 | 2.113 | 2.132 | 2.112 |
| Total $M$ ($\mu_B$) | 0.560 | 0.815 | 1.085 | 1.291 |
| MCA$^1$ (erg/cm$^2$) | −0.344 | 1.136 | 1.025 | 2.503 |
| MCA$^2$ (erg/cm$^2$) | −0.347 | 1.134 | 1.018 | 2.508 |

TABLE II. Values of the total Pt spin magnetic moment and MCA (determined from total energy calculations) for the 5Pt/BTO bilayer for two in-plane lattice constants and two FE polarizations, respectively.

| | 3.920 (Å) | | 3.992 (Å) | |
|---|---|---|---|---|
| 5Pt/BTO | $P_\uparrow$ | $P_\downarrow$ | $P_\uparrow$ | $P_\downarrow$ |
| Total $M$ ($\mu_B$) | 0.463 | 0.940 | 0.404 | 0.719 |
| MCA (erg/cm$^2$) | 0.031 | 0.199 | 0.100 | 0.201 |

netic spin moment of the 5 Pt MLs in the 5Pt/BTO for the two in-plane lattice constants. First and foremost, the ferroelectric polarization of BTO can still induce magnetism in the 5 MLs Pt. In view of the freestanding 5 ML Pt film being nonmagnetic, the onset of magnetism solely arises from the interfacial effect and ferroelectric polarization with BTO. We can see that the layer-resolved spin moments for $a_\parallel = 3.920$ Å (blue bars) are larger than the corresponding moments (red bars) for $a_\parallel = 3.992$ Å for both polarization directions. More specifically, the total Pt spin moments with $a_\parallel = 3.920$ Å are 0.940 and 0.463 $\mu_B$ for $P_\downarrow$ and $P_\uparrow$, respectively, while the corresponding values are 0.719 and 0.404 $\mu_B$ for the bilayer with $a_\parallel = 3.992$ Å. These results, as listed in Table II, demonstrate that the Pt spin moment is proportional to the magnitude of the ferroelectric polarization. However, the magnitude of the spin moments for the 5Pt/BTO decreases substantially compared to the corresponding values in 3Pt/BTO. For example, for $P_\downarrow$ and $a_\parallel = 3.992$ Å the *average* spin magnetic moment reduces from 0.215 $\mu_B$ per Pt atom in the 3Pt/BTO to 0.072 $\mu_B$ per Pt atom in the 5Pt/BTO, indicating that the interfacial and ferroelectric polarization effects on thicker Pt films become weaker. Consequently, the magnetism will finally vanish when the Pt films are thick enough.

To understand the underlying Stoner mechanism of the FE polarization-induced magnetism in ultrathin Pt films and the crucial role of the biaxial strain, we present in Fig. 2(d) the non-spin-polarized average layer-resolved density of states (DOS) without SOC at the Fermi energy, $N(E_F)$, versus in-plane lattice constant for the freestanding 3 ML Pt film (square symbols), where the empty (filled) square symbols represent the nonmagnetic (magnetic) cases. We also display in Fig. 2(d) the non-spin-polarized layer-resolved $N(E_F)$ on the interfacial (I), central (C), and surface (S) Pt layer for the 3 Pt/BTO bilayer (triangles). The black solid line shows approximately the strain-dependent critical value of $N(E_F)$ where the Stoner criterion is fulfilled separating the FM from the nonmagnetic (NM) phase. The fact that this line is not horizontal suggests that the Stoner exchange parameter $I$ depends on strain. Overall, the results reveal that indeed the FE polarization enhances $N(E_F)$ on the surface and central Pt layers compared to that of the freestanding Pt film so that the Stoner criterion is met, thus rendering them magnetic. On the other hand, $N(E_F)$ for the interfacial Pt layer does not satisfy the Stoner criterion, and the smaller magnetic moment presumably arises from the proximity effect from the surface and central layers. It is important to note that the trend of magnetic moments with polarization and strain in Fig. 2(a) is consistent with that of the layer-projected DOS on the surface

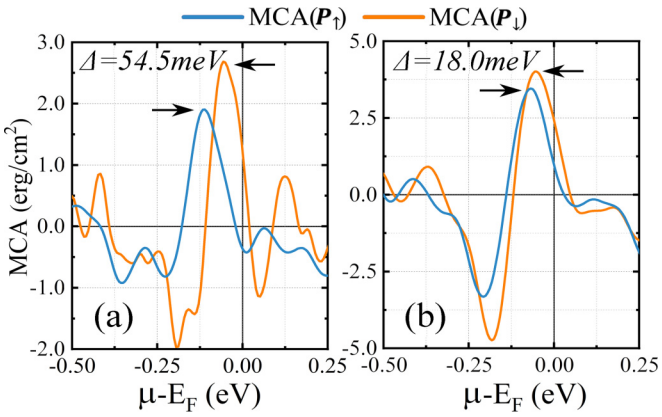


FIG. 3. MCA energy as a function of Fermi level position ($\mu - E_F$) for the Pt/BTO bilayers with $a_\parallel$ = (a) 3.920 and (b) 3.992 Å. Blue and green curves denote the MCA with up and down polarization, respectively. Black arrows show the shift of chemical potential, $\Delta$, upon polarization switching.

and central Pt layers, where $N_S(E_F) > N_C(E_F) > N_I(E_F)$ and the layer-resolved DOS for $P_\downarrow$ is consistently larger than the corresponding value for $P_\uparrow$.

Having established the emergence of FE-induced magnetism in ultrathin Pt films we next investigate the influence of polarization switching on the MCA. The MCA was calculated using two different approaches. The first, discussed above involves total energies. The second employs the force theorem MCA $= \sum_{\mathbf{k}} MA(\mathbf{k})$, where the $k$-resolved MCA($\mathbf{k}$) $\approx \sum_{n\in occ}[\varepsilon(n,\mathbf{k})^{[100]} - \varepsilon(n,\mathbf{k})^{[001]}]$ in the 2D BZ [46,47]. Here, $\varepsilon(n,\mathbf{k})^{[100](001])}$ are the eigenvalues of the Hamiltonian for in-plane (out-of-plane) magnetization orientation. The values of the polarization-dependent MCA of 3Pt/BTO for the two $a_\parallel$ are listed in Table I, where the agreement between the two approaches is excellent. For $a_\parallel = 3.920$ Å the polarization reversal results in magnetization switching from in-plane to out-of-plane orientation, while for $a_\parallel = 3.992$ Å both polarizations favor perpendicular MCA. Nevertheless, for both lattice constants we find a significant *change* of MCA of about 1.5 erg/cm$^2$ under polarization switching ($P_\uparrow \rightarrow P_\downarrow$), which is about a factor of five larger that the reported values for Fe/BTO ($SrTiO_3$) [22,48], indicating a giant electric field MCA efficiency, presumably arising from the large SOC of Pt. Note, that $P_\downarrow$ always gives an enhanced PMA compared to $P_\uparrow$, regardless of the lattice constant. On the other hand, we find that the 5 Pt/BTO bilayer exhibits similar tunable trend of magnetic behavior versus polarization switching, but where the MCA values and their corresponding changes in response to $P_\uparrow \rightarrow P_\downarrow$ are about one order of magnitude smaller than those of the 3Pt/BTO. Hence they are not sufficient in stabilizing the magnetization against thermal fluctuations in practical applications.

To reveal the underlying origin of the changes of MCA upon polarization reversal, taking 3 Pt/BTO as an example, we display in Fig. 3 the variation of the MCA as a function of the shift of chemical potential, $\Delta\mu = \mu - E_F$. The results reveal an overall similar Fermi level dependence of MCA for $P_\uparrow$ and $P_\downarrow$ over a wide range of $\Delta\mu$, suggesting that the change of MCA can be mainly attributed to the rigid shift of the

chemical potential in response to the interfacial repositioning of the Ti and O elements. More specifically, the Fermi level dependence of MCA for $P_\uparrow$ is similar to that of $P_\downarrow$ where $\mu(P_\uparrow) \simeq \mu(P_\downarrow) + \Delta$, namely, involving a rigid shift of the MCA for $P_\downarrow$ to a higher chemical potential $\Delta$. This results from the charge accumulation at the interface for $P_\uparrow$. We find that $\Delta$ is about 54.5 and 18.0 meV for $a_\parallel = 3.920$ and 3.992 Å, respectively, where the different values are due to the different polarization strength induced by strain [22]. Moreover, we have carried out calculations of the electrostatic potential profile normal to the interface for $P_\uparrow$ and $P_\downarrow$, respectively. By calculating the Fermi level with respect to the vacuum level for both polarizations we find $\Delta$ values of 58.8 and 19.2 meV, respectively, which are in good agreement with those obtained from Fig. 3. These results reveal three additional important effects. First, using a FE substrate with larger polarization can enhance even further the efficiency of change MCA via polarization switching. Second, Fig. 3(b) shows that relatively small (<0.15 V) modulation of the chemical potential via gate voltage [33] for example can result both in (i) very large MCA ($\sim$4 erg/cm$^2$) necessary to stabilize magnetic bits (typical MCA values for FeCo/MgO junctions are about 1.2 erg/cm$^2$) and (ii) unprecedented efficiency of magnetization switching solely via gate voltage [49].

The effect of FE polarization switching on the MCA can also be understood from the second-order perturbation theory MCA expression, given by [50]:

$$E_{\mathrm{MCA}} \approx \sum_{I,lmm'\sigma\sigma'} \sum_{o,u} \sigma\sigma' \xi_{Il}^2 \frac{P_u^{Ilm\sigma} P_o^{Ilm'\sigma'}}{E_u^\sigma - E_o^{\sigma'}} \Delta L_{l,mm'}, \quad (1)$$

where

$$\Delta L_{l,mm'} = |\langle lm|\hat{L}_z|lm'\rangle|^2 - |\langle lm|\hat{L}_x|lm'\rangle|^2. \quad (2)$$

Here, $\sigma, \sigma' \equiv \pm 1$ denote the electron spin, $\hat{\xi}$ is a diagonal matrix containing the SOC strength, $\hat{L}_{x(z)}$ is the $x(z)$ component of the orbital angular momentum operator, and $P_n^{Ilm\sigma} = |\langle \Psi_n^\sigma || Ilm\rangle|^2$ is the Bloch wave amplitude projected on atom $I$ (in our case Pt), orbital index $lm$, spin index $\sigma$ and $\Psi_n^\sigma(E_n^\sigma)$ is the one-electron occupied and unoccupied spin-polarized Bloch states (energies) of band index $n$ and wave vector $k$ (omitted for simplicity).

In Fig. 4 we show the minority-spin bands of the surface Pt-derived $d_{yz}$, $d_{xz}$, and $d_{x^2-y^2}$ states for $P_\uparrow$ and $P_\downarrow$, respectively. In contrast to the interfacial states dominated by the hybridization effect, these states are found to yield the dominant contribution to the change of MCA under polarization reversal. Note that the *change* of MCA for 5*d* transition metal thin caps have been found to correlate well to the electric field- or FE-polarization-induced shifts of the *d*-orbital states [22,49]. For $a_\parallel = 3.920$ Å, the occupied surface-Pt $d^\downarrow_{x^2-y^2}$-derived states around $\bar{\Gamma}$ for $P_\downarrow$ shift upward in energy for $P_\uparrow$ and become unoccupied. Consequently, for $P_\uparrow$ this triggers a coupling between the unoccupied $d^\downarrow_{x^2-y^2}$ states and the occupied $d^\downarrow_{yz(xz)}$ states through the in-plane orbital angular momentum operator, $\hat{L}_x$, which in turn yields a negative contribution to the MCA [see Eq. (2)]. This result is consistent with the reduction

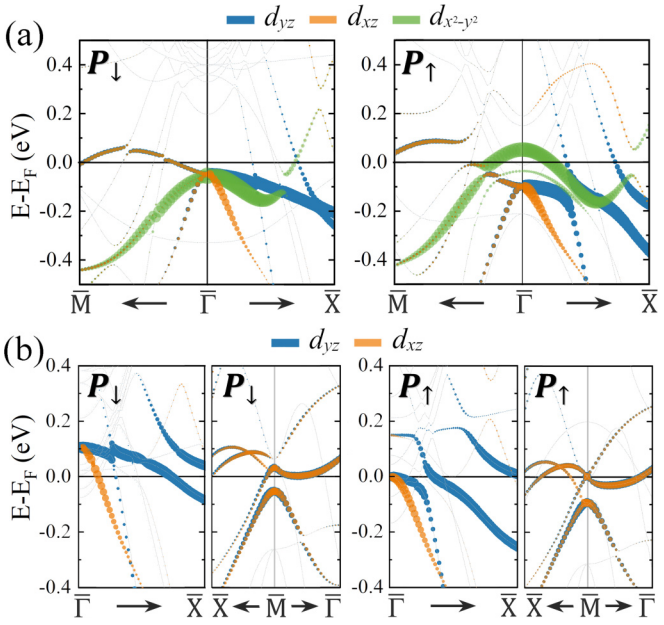


FIG. 4. Energy- and **k**-resolved distribution of the minority-spin bands of the surface Pt-derived $d_{yz}$, $d_{xz}$, and $d_{x^2-y^2}$ states along the symmetry directions of the 2D BZ for $P_\uparrow$ and $P_\downarrow$ and for $a_\parallel =$ (a) 3.920 and (b) 3.992 Å, respectively. The Fermi level is set at zero energy.

of MCA (Table I) under $P_\downarrow \rightarrow P_\uparrow$ switching. For $a_\parallel = 3.992$ Å and $P_\downarrow$ [Fig. 4(b)] the SOC matrix element $\langle d^\downarrow_{xz}|\hat{L}_z|d^\downarrow_{yz}\rangle$ around $\frac{1}{3}\overline{\Gamma X}$ and $\frac{1}{5}\overline{M\Gamma}$ yield positive contributions to the MCA. When the polarization reverses to $P_\downarrow$ the unoccupied $d^\downarrow_{yz}$ states around $\bar{\Gamma}$ and $\bar{M}$, respectively, shift downward in energy and become occupied, thus reducing the MCA.

## IV. CONCLUSIONS

In summary, we report a ferroelectric-driven magnetism in ultrathin Pt films which can also be tuned via biaxial strain. In addition to the modulation of the magnetization, the polarization switching triggers record-high changes of MCA energy compared to the 3*d* FM counterparts, due to the large SOC of Pt. The underlying origin lies on the changes of the chemical potential and hence screening charge induced by the polarization direction. Using a substrate with larger FE polarization can enhance presumably even further the MEC. The FE control of magnetism in ultrathin heavy metals with large SOC may have important implications on the anomalous Hall effect as well as the voltage-controlled magnetic anisotropy in nonvolatile memories.

## ACKNOWLEDGMENTS

We would like to thank M. Coey and A. Ariando for useful discussions. The work is supported by NSF ERC-Translational Applications of Nanoscale Multiferroic Systems (TANMS) Grant No. 1160504 and NSF-Partnership in Research and Education in Materials (PREM) Grant No. DMR-1828019. Q.S. was partially supported by the U.S. Army under Grant No. W911NF-15-1-0066.

[1] N. Spaldin and R. Ramesh, Advances in magnetoelectric multiferroics, Nat. Mater. **18**, 203 (2019).

[2] C. A. F. Vaz, J. Hoffman, C. H. Ahn, and R. Ramesh, Magnetoelectric coupling effects in multiferroic complex oxide composite structures, Adv. Mater. **22**, 2900 (2010).

[3] M. Bibes and A. Barthelemy, Towards a magnetoelectric memory, Nat. Mater. **7**, 425 (2008).

[4] W. Eerenstein, N. D. Mathur, and J. F. Scott, Multiferroic and magnetoelectric materials, Nature (London) **442**, 759 (2006).

[5] J. C. Slonczewski, Current-driven excitation of magnetic multilayers, J. Magn. Magn. Mater. **159**, L1 (1996).

[6] L. Berger, Emission of spin waves by a magnetic multilayer traversed by a current, Phys. Rev. B **54**, 9353 (1996).

[7] I. M. Miron, K. Garello, G. Gaudin, P. J. Zermatten, M. V. Costache, S. Auffret, S. Bandiera, B. Rodmacq, A. Schuhl and P. Gambardella, Perpendicular switching of a single ferromagnetic layer induced by in-plane current injection, Nature (London) **476**, 189 (2011).

[8] L. Liu, C. F. Pai, Y. Li, H. W. Tseng, D. C. Ralph, and R. A. Buhrman, Spin-torque switching with the giant spin Hall effect of tantalum, Science **336**, 555 (2012).

[9] D. Khomskii, Trend: Classifying multiferroics: Mechanisms and effects, Physics **2**, 20 (2009).

[10] G. Radaelli, D. Petti, E. Plekhanov, I. Fina, P. Torelli, B. R. Salles, M. Cantoni, C. Rinaldi, D. Gutiérrez, G. Panaccione, M. Varela, S. Picozzi, J. Fontcuberta, and R. Bertacco, Electric control of magnetism at the Fe/$BaTiO_3$ interface, Nat. Commun. **5**, 3404 (2014).

[11] Q. Sun, Y. Ma, and N. Kioussis, Two-dimensional Dirac spin-gapless semiconductors with tunable perpendicular magnetic anisotropy and a robust quantum anomalous Hall effect, Mater. Horiz. **7**, 2071 (2020).

[12] W. Eerenstein, M. Wiora, J. L. Prieto, J. F. Scott, and N. D. Mathur, Giant sharp and persistent converse magnetoelectric effects in multiferroic epitaxial heterostructures, Nat. Mater. **6**, 348 (2007).

[13] S. Sahoo, S. Polisetty, C. G. Duan, S. S. Jaswal, E. Y. Tsymbal, and C. Binek, Ferroelectric control of magnetism in $BaTiO_3$/Fe heterostructures via interface strain coupling, Phys. Rev. B **76**, 092108 (2007).

[14] S. M. Wu, S. A. Cybart, P. Yu, M. D. Rossell, J. X. Zhang, R. Ramesh, and R. C. Dynes, Reversible electric control of exchange bias in a multiferroic field-effect device, Nat. Mater. **9**, 756 (2010).

[15] D. Pantel, S. Goetze, D. Hesse, and M. Alexe, Reversible electrical switching of spin polarization in multiferroic tunnel junctions, Nat. Mater. **11**, 289 (2012).

[16] Y. Shirahata, T. Nozaki, G. Venkataiah, H. Taniguchi, M. Itoh, and T. Taniyama, Switching of the symmetry of magnetic anisotropy in Fe/$BaTiO_3$ heterostructures, Appl. Phys. Lett. **99**, 022501 (2011).

[17] J. Junquera and P. Ghosez, Critical thickness for ferroelectricity in perovskite ultrathin films, Nature (London) **422**, 506 (2003).

[18] C. A. F. Vaz, J. Hoffman, A.-B. Posadas, and C. H. Ahn, Magnetic anisotropy modulation of magnetite in $Fe_3O_4$/$BaTiO_3$ epitaxial structures, Appl. Phys. Lett. **94**, 022504 (2009).

[19] R. V. Chopdekar and Y. Suzuki, Magnetoelectric coupling in epitaxial $CoFe_2O_4$ on $BaTiO_3$, Appl. Phys. Lett. **89**, 182506 (2006).

[20] H. Zheng, J. Wang, S. E. Lofland, Z. Ma, L. Mohaddes-Ardabili, T. Zhao, L. Salamanca-Riba, S. R. Shinde, S. B. Ogale, F. Bai, D. Viehland, Y. Jia, D. G. Schlom, M. Wuttig, A. Roytburd, and R. Ramesh, Multiferroic $BaTiO_3$-$CoFe_2O_4$ nanostructures, Science **303**, 661 (2004).

[21] J. T. Heron, M. Trassin, K. Ashraf, M. Gajek, Q. He, S. Y. Yang, D. E. Nikonov, Y-H. Chu, S. Salahuddin, and R. Ramesh, Electric-Field-Induced Magnetization Reversal in a Ferromagnet-Multiferroic Heterostructure, Phys. Rev. Lett. **107**, 217202 (2011).

[22] D. Odkhuu and N. Kioussis, Strain-driven electric control of magnetization reversal at multiferroic interfaces, Phys. Rev. B **97**, 094404 (2018).

[23] C.-G. Duan, S. S. Jaswal, and E. Y. Tsymbal, Predicted Magnetoelectric Effect in Fe/$BaTiO_3$ Multilayers: Ferroelectric Control of Magnetism, Phys. Rev. Lett. **97**, 047201 (2006).

[24] C.-G. Duan, J. P. Velev, R. F. Sabirianov, Z. Zhu, J. Chu, S. S. Jaswal, and E. Y. Tsymbal, Surface Magnetoelectric Effect in Ferromagnetic Metal Films, Phys. Rev. Lett. **101**, 137201 (2008).

[25] M. K. Niranjan, J. P. Velev, C. G. Duan, S. S. Jaswal, and E. Y. Tsymbal, Magnetoelectric effect at the $Fe_3O_4$/$BaTiO_3$(001) interface: A first-principles study, Phys. Rev. B **78**, 104405 (2008).

[26] J. M. Rondinelli, M. Stengel, and N. A. Spaldin, Carrier-mediated magnetoelectricity in complex oxide heterostructures, Nat. Nanotechnol. **3**, 46 (2008).

[27] E. C. Stoner, Collective ferromagnetism, Proc. R. Soc. London, Ser. A **165**, 372 (1938).

[28] Y. Sun, J. D. Burton, and E. Y. Tsymbal, Electrically driven magnetism on a Pd thin film, Phys. Rev. B **81**, 064413 (2010).

[29] Y. M. Lu, Y. Choi, C. M. Ortega, X. M. Cheng, J. W. Cai, S. Y. Huang, L. Sun, and C. L. Chien, Pt Magnetic Polarization on $Y_3Fe_5O_{12}$ and Magnetotransport Characteristics, Phys. Rev. Lett. **110**, 147207 (2013).

[30] A. Delin and E. Tosatti, Magnetic phenomena in 5d transition metal nanowires, Phys. Rev. B **68**, 144434 (2003).

[31] S. Kwon, Q. Sun, F. Mahfouzi, Kang L. Wang, P. K. Amiri, and N. Kioussis, Voltage-Controlled Magnetic Anisotropy in Heterostructures with Atomically Thin Heavy Metals, Phys. Rev. Appl. **12**, 044075 (2019).

[32] S. Shimizu, K. S. Takahashi, T. Hatano, M. Kawasaki, Y. Tokura, and Y. Iwasa, Electrically Tunable Anomalous Hall Effect in Pt Thin Films, Phys. Rev. Lett. **111**, 216803 (2013).

[33] L. Liang, Q. Chen, J. Lu, W. Talsma, J. Shan, G. R. Blake, T. T. M. Palstra, and J. Ye, Inducing ferromagnetism and Kondo effect in platinum by paramagnetic ionic gating, Sci. Adv. **4**, eaar2030 (2018).

[34] P. E. Blöchl, Projector augmented-wave method, Phys. Rev. B **50**, 17953 (1994).

[35] G. Kresse and J. Furthmüller, Efficient iterative schemes for ab initio total-energy calculations using a plane-wave basis set, Phys. Rev. B **54**, 11169 (1996).

[36] J. P. Perdew, K. Burke, and M. Ernzerhof, Generalized Gradient Approximation Made Simple, Phys. Rev. Lett. **77**, 3865 (1996).

[37] E. L. Peltzer y Blancá, C. O. Rodríguez, J. Shitu, and D. L. Novikov, Degree of localization of the exchange-correlation hole and its influence on the ground-state (structural and magnetic) properties of d metals, J. Phys.: Condens. Matter **13**, 9463 (2001).

[38] A. H. Romero and M. J. Verstraete, From one to three, exploring the rungs of Jacob's ladder in magnetic alloys, Eur. J. Phys. B **91**, 193 (2018)

[39] J. P. Velev, C. G. Duan, K. D. Belashchenko, S. S. Jaswal, and E. Y. Tsymbal, Effect of Ferroelectricity on Electron Transport in Pt/$BaTiO_3$/Pt Tunnel Junctions, Phys. Rev. Lett. **98**, 137201 (2007)

[40] N. Sai, A. M. Kolpak, and A. M. Rappe, Ferroelectricity in ultrathin perovskite films, Phys. Rev. B **72**, 020101(R) (2005)

[41] G. H. Kwei, A. C. Lawson, S. J. L. Billinge, and S. W. Cheong, Structures of the ferroelectric phases of barium titanate, J. Phys. Chem. **97**, 2368 (1993).

[42] J. P. Velev, C.-G. Duan, J. D. Burton, A. Smogunov, M. K. Niranjan, E. Tosatti, S. S. Jaswal, and E. Y. Tsymbal, Magnetic tunnel junctions with ferroelectric barriers: Prediction of four resistance states from first principles, Nano Lett. **9**, 427 (2009).

[43] M. Stengel, P. Aguado-Puente, N. A. Spaldin, and J. Junquera, Band alignment at metal/ferroelectric interfaces: Insights and artifacts from first principles, Phys. Rev. B **83**, 235112 (2011).

[44] J.-W. Lee, N. Sai, T. Cai, Q. Niu, and A. A. Demkov, Interfacial magnetoelectric coupling in tricomponent superlattices, Phys. Rev. B **81**, 144425 (2010).

[45] F. Zavaliche, H. Zheng, L. Mohaddes-Ardabili, S. Y. Yang, Q. Zhan, P. Shafer, E. Reilly, R. Chopdekar, Y. Jia, P. Wright, D. G. Schlom, Y. Suzuki, and R. Ramesh, Electric field-induced magnetization switching in epitaxial columnar nanostructures, Nano Lett. **5**, 1793 (2005).

[46] J. G. Gay and Roy Richter, Spin Anisotropy of Ferromagnetic Films, Phys. Rev. Lett. **56**, 2728 (1986).

[47] M. Weinert, R. E. Watson, and J. W. Davenport, Total-energy differences and eigenvalue sums, Phys. Rev. B **32**, 2115 (1985).

[48] C.-G. Duan, J. P. Velev, R. F. Sabirianov, W. N. Mei, S. S. Jaswal, and E. Y. Tsymbal, Tailoring magnetic anisotropy at the ferromagnetic/ferroelectric interface, Appl. Phys. Lett. **92**, 122905 (2008).

[49] S. Kwon, P. V. Ong, Q. Sun, F. Mahfouzi, X. Li, K. L. Wang, Y. Kato, H. Yoda, P. K. Amiri, and N. Kioussis, Colossal electric field control of magnetic anisotropy at ferromagnetic interfaces induced by iridium overlayer, Phys. Rev. B **99**, 064434 (2019).

[50] D.-S. Wang, R. Wu, and A. J. Freeman, First-principles theory of surface magnetocrystalline anisotropy and the diatomic-pair model, Phys. Rev. B **47**, 14932 (1993).